Aqueous Glue Setting in Double-Coated Paperboard Systems: The Impact of Application System and Individual Coating Layer Thickness on Glue Bond Formation

Brian Ninness & Greg Welsch, Styron LLC, Midland, Michigan
Don Ventresca, Styron LLC, Petrolia, Ontario
Dave Williams, The Dow Chemical Company, Midland, Michigan

ABSTRACT

In this study, pilot-scale coating trials have been designed and carried out in order to investigate the roles of both the coating application/metering technique and the contribution of individual layer thickness on the bond formation of aqueous glues in double-coated paperboard systems. The coating application systems investigated for the basecoat and topcoat layers comprised the following: Rod/Rod, Rod/Air-Knife, Blade/Air-Knife, Blade/Blade and Film Coater/Air-Knife. The impact of basecoat and topcoat layer thickness was investigated by modifying the two-layer structure as follows: HIGH/LOW, MEDIUM/MEDIUM, LOW/HIGH for each of the above mentioned application systems, whilst maintaining a constant total coat weight.

In addition to standard glue strength testing, an attempt was made to quantify the extent of aqueous glue penetration into the coating layers using both optical and electron microscopy techniques utilizing tracers in the glue. The surface roughness, bulk porosity, and absorption potential of the coating layers were found to be dependent on the application technique; however the impact of individual layer thickness was not observed to be a contributing factor in predicting end-use performance. The use of Laser Scanning Confocal Microscopy with a Rhodamine-B dye in the glue produced the best results for observing the extent of penetration into the coating layers.

INTRODUCTION

Pigmented coatings are applied to paperboard substrates to provide functional properties for beverage packaging and folding cartons, and for enhancement of printing graphics. Latex binders are used in the coatings to provide adhesion to the basesheet and cohesion between the pigments. Additionally for paperboard applications latex binders provide good water resistance to facilitate improved glueability, improve printing press performance, and enhance printability of the coating. The pigmented coating must possess adequate dry and wet strength as this is important for the printing, gluing and converting of the paperboard as well as for final carton use. Since beverage packaging and folding cartons are typically comprised of two or more coating layers, it is critical that the pigmented coatings exhibit adequate layer to layer adhesion as well.

Different coater technology is used to apply pigmented coatings to paperboard, depending on the substrate type, coater speed, and also end use requirements. For example in recycled board mills, coating is typically applied with a series of two rod coaters or a combination of rod and air knife coaters. For bleached board applications used for higher quality printing, the pigmented coatings can be applied by a series of blade coaters or a combination of blade, rod, or air knife coaters. For coated unbleached kraft board applications, various combinations of these are employed.

Each coating application technology has advantages and disadvantages from a coating structure perspective for paperboard.[1,2,3] Blade coaters will produce coatings with high smoothness, but the consistency of the coating thickness will depend on the smoothness of the substrate. Because of the high pressure impact with blade coaters, there is significant orientation of the pigment particles as they flow under the blade tip. Rod coaters are typically used in low speed applications and will produce a fairly smooth surface but, like the blade coater, the consistency of the coating thickness will depend on the smoothness of the substrate. Lower unit pressure for the rod versus the blade is realized but some orientation of the pigment particles will likely occur. Air knife coaters produce a perfect contour coating, thus coating thickness is very consistent, but smoothness is not good. The alignment of pigment particles tends to be more random with this type of coater. Film coaters produce a contour smoothened coating, so the coating thickness uniformity is in between blade and air knife coaters. Film coating does not produce a smooth surface due to film split effects such as orange peel.

In this study pilot-scale coating experiments have been designed and carried out in order to investigate the roles of both the choice of coating application technique and the contribution of individual layer thickness on the bond formation of aqueous glues in double-coated paperboard systems. The coating metering systems used in this study for the basecoat and topcoat layers comprised the following: Rod/Rod, Rod/Air-Knife, Blade/Blade, Blade/Air-Knife and Film Coater/Air-Knife. The impact of coating layer thickness was investigated by modifying the two-layer structure and coat weight split as follows: HIGH/LOW, MEDIUM/MEDIUM, LOW/HIGH for each of the above mentioned application systems with total coat weight remaining constant.

EXPERIMENTAL

The coating formulations used in this study are described in TABLE 1. These formulations were chosen as a general representation for a recycled board or unbleached kraft board coating.

Formulations	Basecoat	Topcoat	Topcoat (air knife)
	parts	parts	parts
#1 Clay	77	65	65
Calcined Clay	23	20	20
TiO_2		15	15
SB Latex	14	17	17
Thickener	0.5	0.5	0.5
Solids (%)	64	60	46
pH	8.5	8.5	8.5

TABLE 1: Basecoat & Topcoat Formulations.

Due to the requirements for a low viscosity coating, the air-knife coating solids was reduced to ensure good runnability with this metering technique. Although these formulations are typically used for recycled or unbleached kraft board, the formulations were applied onto 10 point bleached board at the Styron Pilot Coater in Midland, MI. This decision was made in order to give longer run time (lower caliper substrate with more footage per roll) to achieve constant coat weight values at coat weight target to insure good experimental results. The coater combinations used in the study are described in TABLE 2. Each of these represent application combinations currently employed in the production of double coated paperboard with the possible exception of the film coater/ air knife combination. This combination was added to evaluate a non typical application system.

Basecoat Coating Method	Topcoat Coating Method
Rigid Blade	Rigid Blade
Rigid Blade	Air Knife
Rod	Rod
Rod	Air Knife
Film Coater	Air Knife

TABLE 2: Coater Combinations used for during pilot trial.

Coating speed for both basecoat and topcoat applications was constant at 900 fpm (274 mpm), with a consistent basestock moisture of 5.3% (+/- 0,2 %). The drying configuration consisted of a combination of both IR and air-flotation. The total coat weight target was 5.0 lbs/1000 ft^2 (24 g/m^2), and was split between the basecoat and topcoat according to TABLE 3.

	% Basecoat Target	Basecoat (Range) (lbs./1000 ft^2)	% Topcoat Target	Topcoat (Range) (lbs./1000 ft^2)
Spl1	40	1.75 (+/- 0.15)	60	3.00 (+/- 0.30)
Spl2	50	2.65 (+/- 0.25)	50	2.35 (+/- 0.15)
Spl3	60	3.00 (+/- 0.30)	40	1.90 (+/- 0.50)

TABLE 3: Sample Designation & Coat Weight Split.

RESULTS & DISCUSSION

The ability of coated paperboard to set an aqueous glue in a process-realistic time and to sustain a strong glue bond is of paramount importance in the converting process. The primary objective in this study was therefore to attempt to relate the gluing performance of the coated board to the coating structure development caused by the differing application techniques. For aqueous glues the mechanism of setting and bond formation necessitates that the glue dewaters, with the aqueous mobile phase being able to penetrate through the coating layers and enter the fibre matrix. Most manufacturers of coated paperboard use in-house qualitative test procedures to ascertain the extent of glue-bond formation. These tests typically comprise one of two methods; (1) the measurement of the time required to reach 100% fibre tear or (2) the extent of fibre tear after a specified period of time. To achieve acceptable and consistent fibre tear the weakest link within the system must be the fibre-fibre bond of the substrate. Coating layer and/or adhesive layer failure is not acceptable.

Coating Layer Morphology

The morphology of the coating layer should have a direct impact on both the setting of the aqueous adhesives and the formation of the final adhesive bond. Standard board testing for roughness (PPS) and porosity (Hagerty) were conducted in order to observe the effect of application technique on the final coating structure morphology. In addition the development of the fine pore structure induced by the various application systems was investigated using mercury intrusion porosimetry. Finally, the short-time absorption potential of the samples was investigated using the Bristow Wheel test.

PPS Roughness. The PPS roughness of the basecoats and the double-coated samples can be found in FIGURES 1 and 2 respectively. The basecoat data shows that the Film-Coater produces by far the roughest surface, with barely any improvement in smoothness over the basestock itself. The blade coater produces the smoothest surface with the rod coater slightly higher in roughness. The effect of coat weight on the smoothness development for the blade and rod coaters is also evident as the basecoat coat weight is increased from Spl1 to Spl3. The double coated samples have the same trend with the Blade/Blade combination producing the smoothest coating and the Film-Coater/Air-Knife combination the roughest. In fact, this combination produced a surface roughness only slightly better than the base sheet itself. Modeling of the double coated PPS data gave strong correlations, with R^2 of 0.95. The significant variables were the basecoat blade coater (reduced PPS) and the basecoat film coater (increased PPS).

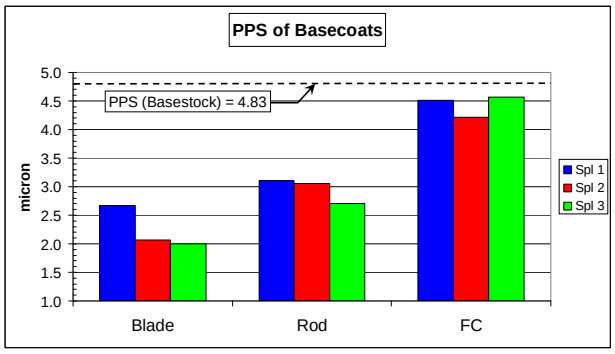

FIGURE 1: PPS Roughness of the Basecoats.

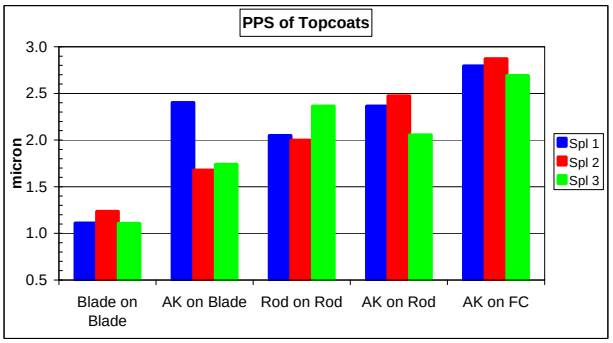

FIGURE 2: PPS Roughness of the Topcoats.

Hagerty Porosity. Coating porosity was measured on the basecoats and the double-coated board using the Hagerty Permeability method. The basecoat results are given in FIGURE 3 and indicate that the porosity of the basecoats very much depends on the choice of application system. The blade-coated samples show the least porosity, followed by the rod-coated samples, and the film-coated samples exhibit the highest porosity (lowest value). It is also evident, especially for the blade and rod sample that as the CW is increased, moving from Spl1 to Spl3, the porosity decreased as expected. The results are typical of clay-based formulations where the metering step has a pronounced impact on the alignment of the pigment particles. The porosity is decreased as the clay platelets are aligned in the shear field under the blade and are able to pack more closely. The shear field being highest under the tip of a rigid blade, followed by the smooth rod, and finally to the more random particle orientation produced by the film-split of the film-coater.

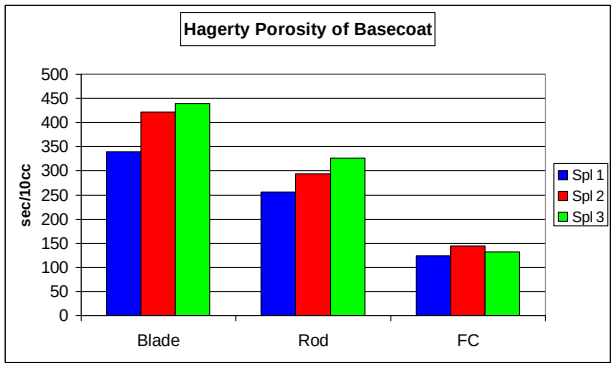

FIGURE 3: Hagerty Porosity of Basecoats
(Lower value = higher porosity).

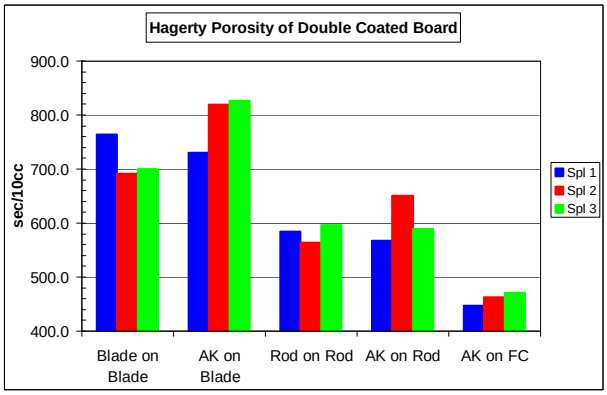

FIGURE 4: Hagerty Porosity of Double-Coated Board
(Lower value = higher porosity).

The Hagerty results of the double-coated systems are given in FIGURE 4, and systematically show a decrease (higher value) in overall porosity as compared to the basecoat-only samples as expected. The data indicates that the porosity of the double-coated structure is strongly influenced by the base coat application and has the same ranking as that of the underlying basecoats. Regression modeling of the double-coated porosity data produced a model with R^2 of 0.96, with basecoat blade (decreased porosity) and topcoat air knife (increased porosity) coater techniques as the significant variables.

Comment [GW1]: Not sure if this statement is accurate so I struck it out.

Comment [BN2]: need to check this

Mercury Porosimetry. Mercury Porosimetry (Micromeritics Autopore III) was used to characterize the pore size distribution of the various samples. Weighed samples are placed in the device and vacuum conditions applied for 20 minutes to ensure the samples are evacuated. Low pressures are used to apply and press the mercury into the large pores (basestock) while higher pressures are used to reach the smaller pore sizes of the coating structure. The volume of mercury penetrating the sample is accurately measured. The pressure required is converted to an equivalent pore size using the Laplace equation and the surface tension of mercury (assuming a contact angle of zero). The Spl 2coat weight samples (MEDIUM/MEDIUM) of each coater combination was analyzed. FIGURE 5 illustrates the log differential in pore volume of the five double-coated samples. By looking at the log-differential plot we can see the two major pore size categories; paper pores (1 – 10 µm) and those pores associated with the

coating structure (0.05 – 0.10 µm). This plot shows that the vast majority of pore volume is due to the paper substrate; however the coating pores are distinct.

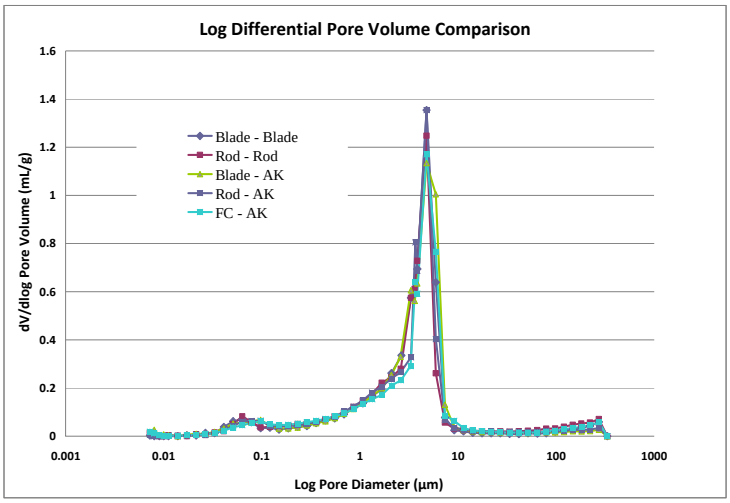

FIGURE 5: Log-Differential Pore Volume of Double Coated Samples.

FIGURE 6 shows the enlargement of the coating pore size range. For these samples the coating formulations were the same, and the final coat weight also constant. Therefore the difference in application method does show some shifting of the pore size distribution. All of the samples with an air-knife topcoat show a consistent and significant increase in the coating pore size. This result indicates that the air-knife application method tends to generate a larger pore in the coating structure than either the rod or blade applied topcoats. This could be attributed to the lower shear or compression of the coating layer during application leaving the pigment particles randomly distributed, and also due to the difference in consolidation caused by the required lower solids content of the air-knife formulation.

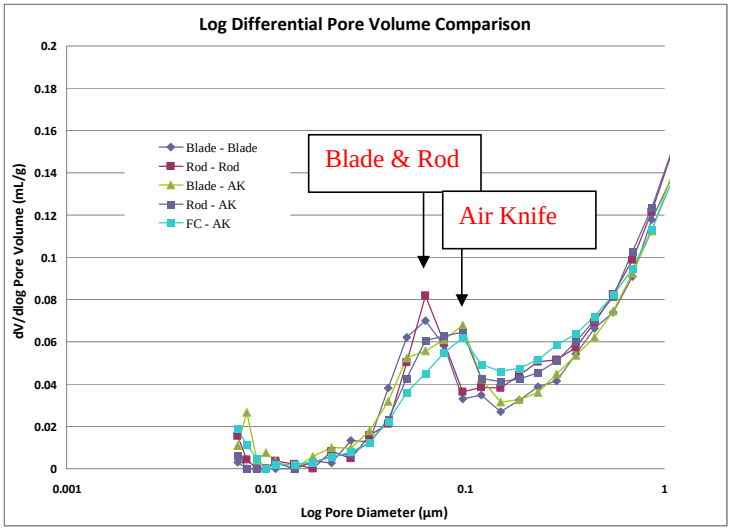

FIGURE 6: Log-Differential Pore Volume in the Coating Pore Size Regime.

The five double-coated samples represented in FIGURES 5 and 6 all contain one of three applied basecoats (Blade, Rod, Film-Coater). One method to attempt to characterize the topcoat layer's pore structure is to subtract the pore volume of the basecoat samples from those of the corresponding double-coated samples. FIGURE 7 represents the log-differential pore volume of the basecoat-only samples. The results here again show a difference in the coating pore size due to the application method (formulation and coat weight are constant), The Blade coated basecoat shows the smallest pores, while the Film-Coater tends to generate more pore volume and at a larger pore size.

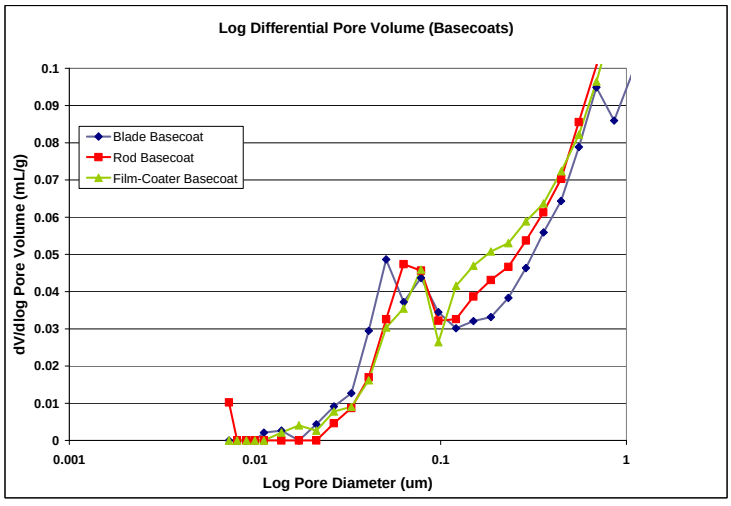

FIGURE 7: Log-Differential Pore Volume of Basecoats.

By subtracting the pore volume of the basecoat (FIGURE 7) from that of the double-coated samples (FIGURE 6), in theory we should be able to arrive at the contribution to the cumulative pore volume just due to the final topcoat layer. In practice, however, a few issues need to be considered that may make this hypothesis not entirely accurate. For example, if some of the coating pigments or binders from the topcoat layer begin to fill up voids in the basecoat, a reduction of pore volume would be obtained. FIGURE 8 demonstrates the result of this subtraction for the coating pore sizes below one micron in size. The differences in these curves are significant, and again demonstrate that the application method does have measurable effect on the coating structure's pore volume. The Rod – Rod and Blade – Blade samples yield almost identically shaped pore volume curves, while the Air-Knife topcoats are grouped together. Again, we must take into account the influencing factors that may alter the results of the subtraction method, namely coat weight variations and pore filling. Based on the Hg porosimetry data presented in FIGURES 5 – 8, and considering the bulk porosity data obtained via the Hagerty test, it is evident that the application method results in changes in the pore structure of the final consolidated coating structure.

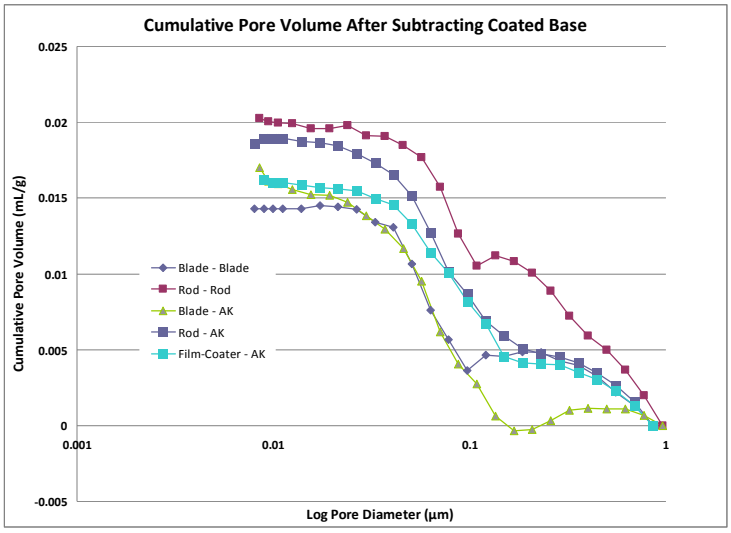

FIGURE 8: Cumulative Pore Volume of Topcoat Layer.

Bristow Absorption Test. The Bristow Absorption Test was used to investigate the short-time liquid absorption properties of the samples. The unit consists of a rotating wheel which can be run at various, fixed rotational speeds. The substrate is attached to this wheel, and a known volume of fluid is held within the trough. As the substrate moves under the liquid trough the liquid is transferred to the surface of the substrate. The rate of absorption can then be calculated from the area of the liquid trace, the speed of the wheel and the volume of fluid applied. We utilized speeds of 0.1, 1.0 and 5.0 cm/sec, which corresponded to contact times of 1.0, 0.1, and 0.02 sec respectively. For this study a diluted, water-based inkjet ink was used as the fluid. The data shown here represents the total liquid volume transferred to the substrates at a contact time of 0.1 sec. The complete data set is available in Appendix A.

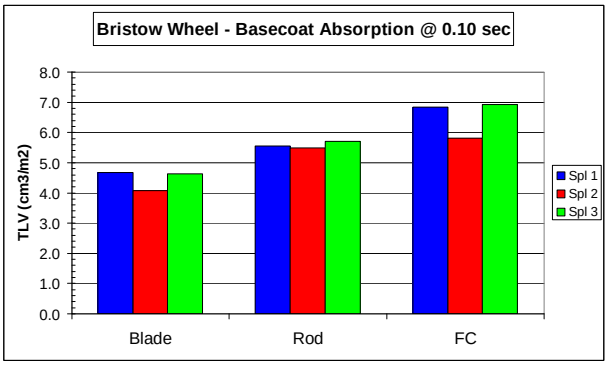

FIGURE 9: Bristow Wheel Absorption (basecoats).

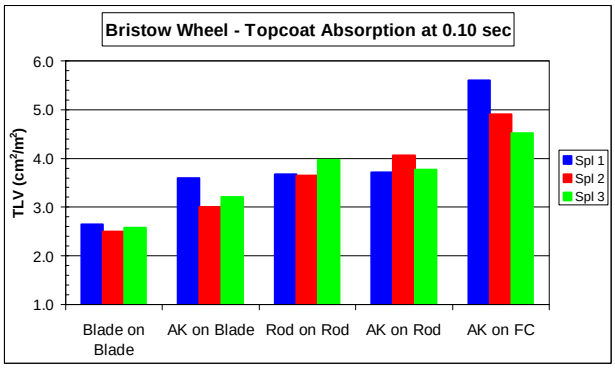

FIGURE 10: Bristow Wheel Absorption (topcoats).

Bristow Wheel absorption data at 0.10 seconds contact time for the basecoats and the topcoats can be found in FIGURE 9 and FIGURE 10 respectively. Slowest absorption was observed with the blade coated basecoats and highest absorption with the film coated basecoat The data shows that the double-coated samples exhibit lower absorption than the basecoats, regardless of coater type. For the contour structure provided by the Film-Coater/Air-Knife combination, more uniform coating thickness likely results in lower basesheet effects. The Bristow data of the double-coated systems correlates very well with the Hagerty porosity data given in FIGURE 4. Modeling of the Bristow data for the topcoats at 0.10 seconds gave strong correlations, with R^2 of 0.94. The significant variables were the basecoat blade coater (decreased volume absorbed), the basecoat film coater (increased volume absorbed) and the topcoat blade coater (decreased volume absorbed). Thus the most absorptive system is the air knife over the film coater, with the film coater having the dominant effect.

Glue Strength Testing

Two glue testing protocols were conducted on the double-coated board samples, utilizing two different glues. The first aqueous glue setting test is conducted using a 37% solids, polyvinyl acetate acrylic copolymer liquid adhesive (The Reynolds Company). The glue is applied to the double-coated surface using a 0.38 mm bird bar, and the backside of the sample is brought into contact with the glue layer. A three pound steel plate is placed on top of the glued sample and removed after a three minute dwell time. The % fiber tear is evaluated visually after separating the glue joint after 1 and 2 hours of drying. The ideal target is to achieve 90 – 100% fiber tear in the separated sample. The results of this first test are summarized in FIGURES 11 and 12.

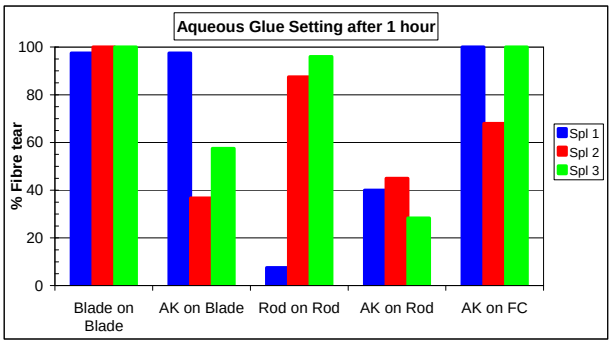

FIGURE 11: Aqueous Glue Strength after 1 hour setting time.

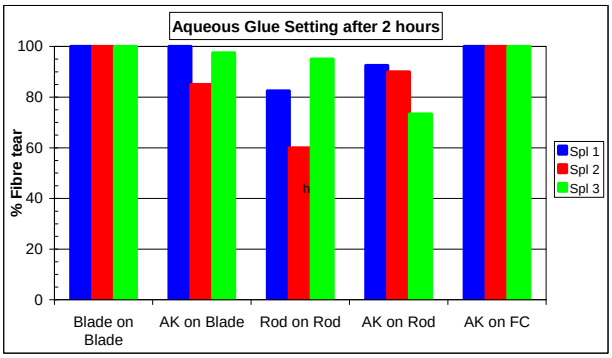

FIGURE 12: Aqueous Glue Strength after 2 hours setting time.

The data shows that the blade/blade combination produces a coating with fast glue setting and good final glue strength, regardless of the coat weight split ratio. The fast set time is surprising considering that the porosity and absorption testing indicates that this combination yields the least porous coating structure Perhaps a higher number of small capillary-type pores may exist that increase the transport of the aqueous component of the glue through the coating. Another potential cause for this observation may be the thinner coat weight areas which exist due to the blade coating method, which may allow faster transport of the mobile phase of the applied glue. The Film-Coater/Air-Knife combination, which produced the most porous coating (by Hagerty measurements), also had fast glue set time and good final glue strength. Overall, all of the combinations with rod basecoats gave slower glue set time. The slowest was with the Rod/Air-Knife combination.

Kellogg Glue Test. The second glue test was conducted in order to look at the shorter timescale glue setting phenomena. The Kellogg glue test is a standard test methodology used extensively in the coated recycle board industry. The aim is to investigate how rapidly the bonding force builds up between two paperboard sample strips once glued together. A shorter time for a sample to exhibit substantial fiber tear is an indication of the glue setting time. By keeping the glue and basestock consistent, the effect of the coating layer(s) on the glueability can be evaluated. For this test a 57% solids, polyvinyl acetate liquid adhesive (Capital Adhesives) was utilized. A glue-film thickness of 15 mils (3 inches wide) is applied to the double-coated side using a Bird film applicator, and immediately the second paperboard sample (backside) is placed on top of the glue film. A 5 lb. steel roller is passed over the sample once in the forward direction and once again in the reverse direction. A timer is started once the steel roller has been removed, and the glued strip is pulled back at specific time intervals and the degree of bond is

determined visually. Once the strip breaks, or a deep glue bond is noted with at least 50% fiber tear across the strip, the time is noted as the final result.

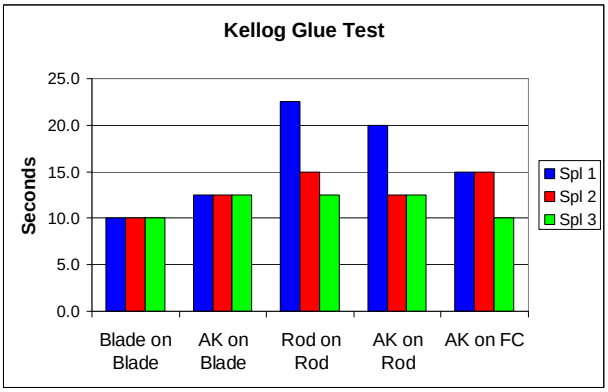

FIGURE 13: Kellogg Glue Test Results

The results of the Kellogg glue test are shown in FIGURE 13. The data correlates well with the 1-hour glue test results given previously in FIGURE 11, specifically showing that the Blade/Blade samples, regardless of the split in coat weight, shows the fastest glue set time. The results for each of the coater combinations shows, with the exception of the Rod basecoats, that the glue set time seems to be independent of the split in the coat weight between the basecoat and topcoat. The low coat weight, rod applied basecoat (Spl 1) shows both the longest time to reach fiber tear in the Kellogg test as well as weak final glue-bond strength after 1 hour in the aqueous glue test.

Glue Penetration via Microscopy

It has been well studied and documented that the choice of coating application system impacts the overall structure of the consolidated coating layer.[1 – 3] In addition, this final coating structure, as it relates to the pore size, pore size distribution and surface topography, has a direct impact on the setting of aqueous-based glue systems. The mechanism of aqueous-based glue setting necessitates that the vehicle portion of the glue be able to penetrate and pass through the coating layer(s) and enter the fiber network where the moisture can be absorbed. Therefore it stands to reason that the consolidated coating's morphology, as it relates to pore structure, surface roughness and absorption potential should have a direct impact on the ability to form a strong glue bond (100% fiber tear) at the upper most layer.

There have been various attempts using tracers and different analytical techniques to monitor the liquid-phase movement of inks, glues, and coatings. Researchers have tagged glue with OBA and attempted to follow the liquid penetration with a fluorescent lighting SEM technique.[4] In this case coated board which demonstrated good fiber tear was shown to have glue-vehicle penetration down to the coating/fiber interface. Various metallic compounds (oxides and carboxylates) have been added to ink and glue systems in order to monitor the movement or transfer of these liquid systems after application. Trace metal carboxylates were added to gravure inks and ink mileage determined by monitoring the ink transfer via Inductively Coupled Argon Plasma (ICP), Atomic Emission Spectroscopy (AES).[5] In an attempt to measure the CD glue profile researchers employed the use of trace amounts of metallic oxides (iron and zinc) in the glue, and measured the profile using X-ray fluorescence.[6] The determination of ink vehicle penetration has also been studied using laser scanning confocal microscopy using a dye based ink.[7]

The mechanism of aqueous-based glue setting necessitates that the liquid-phase portion of the glue be able to penetrate the coating layer, and also the backside of the substrate, in order to dewater the glue, set it and form the final bond. In an attempt to correlate the aqueous-glue setting results with the varying degree of attained coating structure, three microscopy techniques were utilized that combined some of the attributes from the tracer work described above.

SEM with metal oxide nanoparticles as tracer. Very small (< 25 nm), monodisperse metallic oxide particles were investigated as tracer materials for the aqueous glue. It was hypothesized that these particles would be small enough to penetrate the porous network of the coating structure with the liquid vehicle of the glue, and allow monitoring of the depth of penetration. The following metal-oxides were initially investigated as they were commercially available, of the appropriate size, and posses unique and distinguishing X-ray emission lines; Fe_2O_3, CeO_2, and ZnO. It was quickly realized that iron is a poor choice of a tracer material as both the fiber matrix and the coating pigments contained sufficient amounts of iron contamination. Therefore the development of this technique proceeded using the cerium oxide (CeO_2) as the tracer material, which was obtained from Aldrich as a 10 wt% dispersion in water, with a maximum particle size of 25 nm.

The 37% solids content polyvinyl acetate (PVAC) glue was doped with 1% by wt. of the CeO_2 and the glue applied in the same manner as outlined in the aqueous glue setting test method. A portion of each sample was embedded in epoxy resin and metallographically polished. Backscatter images of the cross sections of the glued board were obtained. In all cases the x-ray mapping revealed no migration of the nanoparticles from the glue. As a confirmation that these tracers do not enter the coating structure a second experiment was performed in which a pure dispersion of the particles was applied to the coated board. A 5% w/w dispersion of the CeO_2 in water was applied to the surface of the Blade/Blade sample (Spl3) using a 3 mil bird bar. After drying at room temperature the sample was cross-sectioned, polished and x-ray mapped.

FIGURE 14 shows the SEM elemental mapping of the double coated system with the CeO_2 layer applied to the surface. The double coated layers are easily observed in the back scatter electron (BSE) image of the upper left quadrant. The delineation of the base and top layers is made apparent by the presence of TiO_2 in the topcoat. It is even more apparent that the applied CeO_2 dispersion has produced a uniform and dense layer of particles at the surface of the coating, with no indication that the small particles have entered the porous structure of the top coating layer. As confirmation that the metal oxide particles are unable to penetrate the coating layer, elemental x-ray spectra were collected of the surface oxide layer in addition to the first few microns of the coating layer. The elemental x-ray map and the corresponding spectra are given in FIGURE 15. The green spectrum in FIGURE 15 was acquired from the green box on the cross sectional image, and clearly shows the strong x-ray line from the cerium. The blue spectra was acquired from the yellow box (topcoat layer) on the image, and clearly shows the large signal due to TiO_2, but also the lack of any signal due to the CeO_2.

Considering the dominant pore size of the coating layers is 100 – 1000 nm, as measured by Hg porosimetry, it was hypothesized that the 25 nm CeO_2 particles would migrate to a certain extent into the coating structure. It is believed that upon drying the oxide particles aggregate into clusters that bridge the surface pores, resulting in the dense filtercake observed in the SEM images of FIGURE 14. Although the metal oxide, tracer SEM technique did not allow us to monitor aqueous-glue penetration, the refinement of this technique however may prove valuable to other research work in the coating area. The small nanoparticles of metallic oxides demonstrate strong and unique X-ray emission lines even when present at very low concentrations.

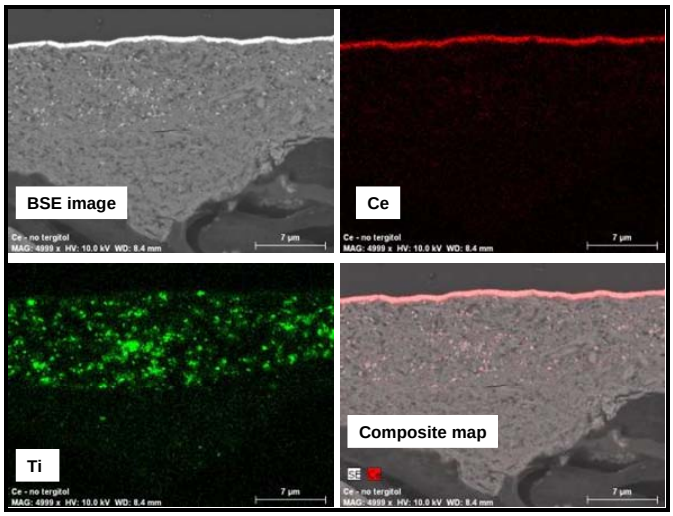

FIGURE 14: SEM Elemental Maps of the Blade/Blade sample with the CeO_2 Dispersion applied to the Surface.

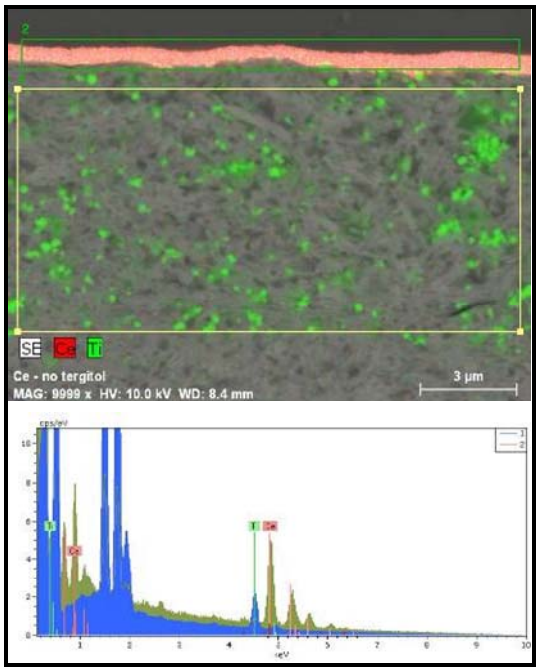

FIGURE 15: (A): Elemental Map, (B) Corresponding Spectra.

Laser Scanning Confocal Microscopy. The aqueous glue was stained with Rhodamine–B dye, building on techniques described by Ozaki et al.[7-9] The key idea here is that the thickness of the glue layer, as imaged by the microscope, will give a quantitative measure of the glue penetration into the coating layer. The Spl2 sample (medium basecoat – medium topcoat) from each set of coater combinations was imaged using this technique. The testing was performed several days after glue application; therefore it is assumed that all migration had concluded before imaging was begun. Images were obtained on the physical cross-sections using a Confocal Laser Scanning Microscope (Leica TCS-SP2) equipped with a 40x air objective lens. The confocal technique can be used to obtain optical cross-sections by using a higher resolution oil-immersion lens, however sample handling and preparation issues become an issue. For the confocal technique the glued sample needed to be torn apart and the confocal image taken from the side that did not tear. The images taken in this manner produced a "smeared" appearance in the z-direction, and therefore the analysis continued only with the physical cross-sections. An excitation wavelength of 514 nm from an Argon laser (Power: 50 mW) was used, along with a beam-splitter that separates the fluorescent wavelength from the excitation wavelength. The pinhole diameter was set to 50 µm. The detected wavelengths ranged from 535 nm to 680 nm, as the emission wavelengths of the Rhodamine dye was from 535 to 680 nm.

Sample preparation proved to be quite critical in obtaining artifact-free images and in maintaining the integrity of the glued samples. As a first attempt a portion of each sample was embedded in epoxy resin, and cross sections were polished (in the direction parallel to the glue layer) using a Reichert-Jung Ultracut E microtome equipped with a glass knife. This sample-prep process provided uniform and flat cross sections. However in a majority of the samples this polishing sequence caused delamination of the glue and/or coating layer. As an example FIGURE 16 illustrates the resulting image obtained from the Blade/Blade sample. The glue layer can be seen to have separated from the coating layers in different locations. The results however were promising, as it can be seen that a portion of the Rhodamine-B dye has penetrated into the coating layers on both sides of the applied glue.

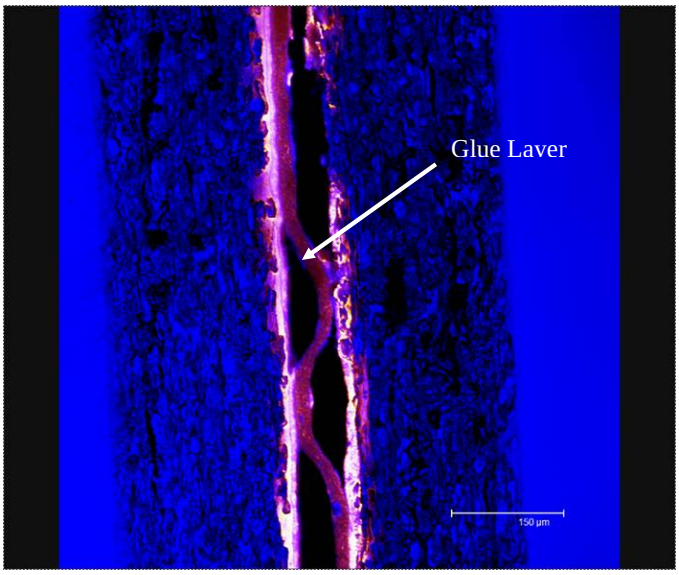

FIGURE 16. CLSM Image of Blade/Blade Sample using Epoxy Embedding and Microtome Polishing.

Based on the results from the epoxy embedding process it was decided to proceed by preparing microtome cross sections without the epoxy embedding process. FIGURE 17 exhibits the images obtained from the five different coater combinations. The length scale-bar in the images is 150 µm. The glue layer, and/or any portion of the glue vehicle, which contains the Rhodamine dye shows up in fluorescence. The blue color represents reflected light. In an attempt to quantify the degree of glue penetration, a series of 15 measurements are taken on each image, as illustrated by the horizontal lines in the Blade/Blade image. In this fashion the width of the fluorescent region can be quantified. Measurement results for all configurations are summarized in TABLE 4.

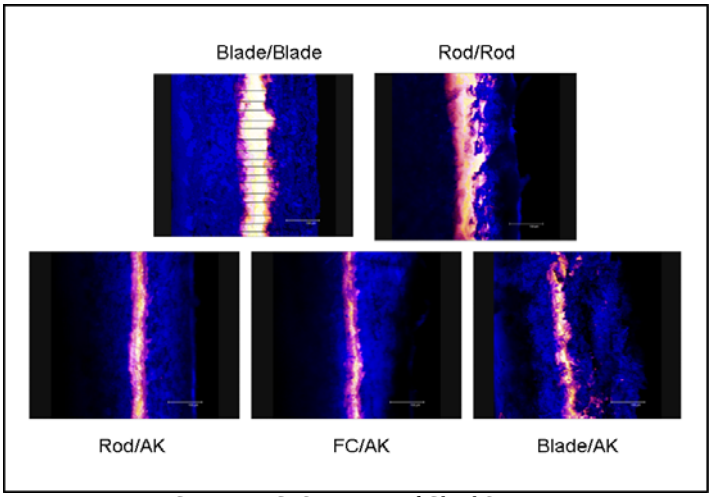

FIGURE 17: CLSM Images of Glued Systems.

SAMPLE	Avg. Width (microns)	Std. Dev.
Blade - Blade	145	21
Rod - Rod	141	33
Blade – Air Knife	81	49
Rod – Air Knife	69	7
Film Coater – Air Knife	61	9

TABLE 4: Width Measurements of Glue Layer (Rhodamine – B).

There seems to be a significant variation in the width of the imaged glue layer for the different coated samples. In theory, since the same amount of glue was applied, using the same glue application technique, the only difference from these images should be due to the differing degrees of glue/vehicle penetration. A thin florescent region would indicate little to no migration of the glue into the coating layers, whereas a wider line indicates migration away from the glue layer and into the surrounding coating structure. It is evident from the images and their respective measurements that the double-coated samples with an Air Knife applied topcoat exhibit a much thinner fluorescent region, indicating much less penetration into the coating structure.

The average thickness of the dried glue layer for the Blade/Blade samples can be seen from the SEM image in FIGURE 18 to be roughly 25 – 30 µm, with the composite coating/glue structure to be roughly 50 – 100 µm thick.. The fluorescent imaging technique therefore suggests that a portion of the aqueous glue is able to penetrate completely through the coating structure and into the fiber matrix.

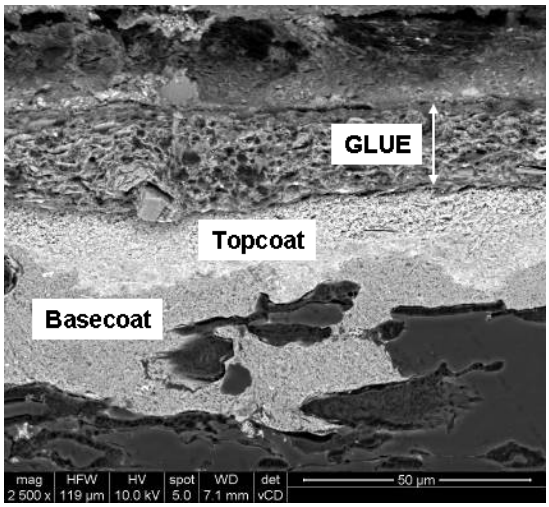

FIGURE 18: SEM Image of Blade/Blade Sample with Glue.

Optical Microscopy. As demonstrated in FIGURE 16, the epoxy embedding and mechanical polishing procedure tended to cause delamination of the glue layer. Mechanical methods of preparing cross sections of composite materials that contain both hard and soft components can be difficult. These methods can be time-consuming and can introduce artifacts in soft materials, deform the material around voids, or compress layers of soft and hard materials.[10] Also, in order for optical microscopy techniques to be useful a truly flat cross section is required. Therefore an attempt was made to utilize an ion beam cross section polisher (JEOL Ion Cross Section Polisher) to prepare the samples. This method does not require the sample to be embedded in epoxy, and is typically used when the epoxy matrix may cause disturbances to the sample itself. The JEOL ion polisher consists of a specimen chamber with a turbo pump vacuum system, and an optical microscope for specimen positioning. The polishing speed is approximately 100 µm/hour, and with the ability of the specimen to be rocked ± 30º to prevent beam striations. The Film Coater – Air Knife sample was polished using this procedure and the image obtained is shown in FIGURE 19. The image was acquired at 50x magnification using a Zeiss Axio optical microscope equipped with dark field illumination. Due to the thickness of the sample the polishing time necessary was roughly 24 hours. As can be seen the polishing procedure still produced ion beam striations in the cross section. However, it is still evident that the Rhodamine-B dye has effectively migrated from the applied glue layer, through the backside and topside coatings, and entered the fiber matrix.

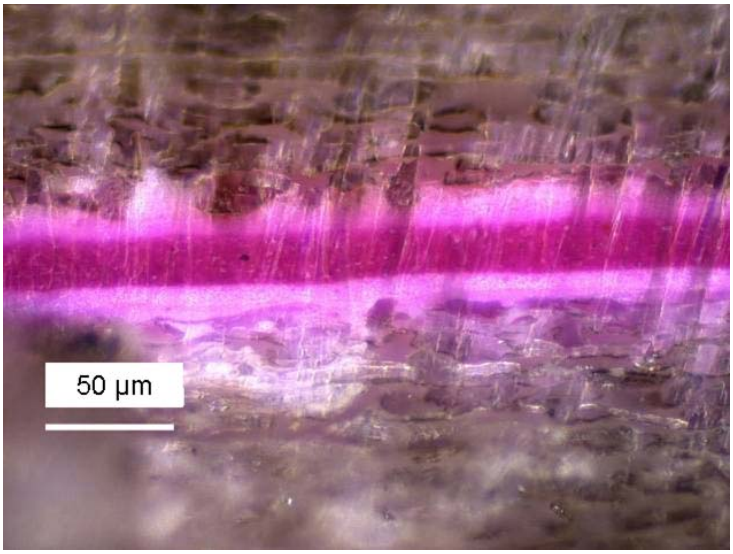

FIGURE 19: Optical Microscopy Image of FC – AK Sample prepared using Ion Beam Polishing.

CONCLUSIONS

The pilot coater prepared samples and the corresponding test results confirm the general knowledge that the choice of application system has a direct impact on the consolidated structure of the coating layer. Blade coating is shown to produce a smooth, less porous structure than that of the true contour coating methods such as the film-coater and air knife. The split of the applied coat weight between basecoat and topcoat is less impactful when the same application technique is used for both (Blade – Blade & Rod – Rod), as compared to the use of two different application methods (Blade – Air Knife). The thickness of the topcoat applied air-knife layer has a direct impact on the final structure and hence its end-use performance.

It has been shown that the air-knife applied topcoat produces a slightly different pore structure, resulting in larger coating pores than the blade or rod topcoats. Generally speaking as the thickness of the air-knife topcoat layer is increased we observe a decrease in smoothness, an increase in porosity, and a faster rate of water uptake. These changes in the coating structure also manifest themselves into a slightly better glue setting performance as the air-knife layer is increased in thickness.

Overall the best performing double-layer system with regards to glue setting and final bond strength is that with the blade applied basecoat and blade applied topcoat. Although this system exhibits the least porous nature as measured by both air leak methods (Hagerty) and also mercury porosimetry, the CLSM image shows that this system also demonstrates the most extensive penetration of the glue vehicle. A larger number of small capillary pores may be the driving force for enhanced penetration, although we must also consider that the interfacial smoothness may also play a dominant role.

It is well known that modifications to the coating formulation (pigment morphology, binder level, etc.) can have dramatic effects on the structure of the consolidated coating layer, and hence its performance in promoting rapid setting and final glue bond strength. Here we have demonstrated also that the choice of application technique must be considered when glue performance is of paramount importance. Although the majority of glue testing procedures are semi-quantitative in nature at best, and exhibit a great deal of variability, they do provide the paperboard manufacturer with a predictive quality control tool. The research area encompassing glue setting and penetration is still evolving, however we see great utility in the continuing evolvement of analytical techniques that allow the penetration of the glue to be monitored and quantified.

ACKNOWLEDGEMENTS

We would like to thank Styron LLC for allowing us to present this paper. Also, the authors would like to express their gratitude to Professor Doug Bousfield for assistance with the Bristow wheel, Confocal Laser Scanning Microscopy, and Mercury Porosimetry testing. Additionally, the efforts of the staff members at the Emulsion Polymers TS&D testing labs are greatly appreciated, especially Sandy Umphrey for organizing the vast amounts of samples and respective testing.

REFERENCES

1. Salminen, P., Yang, A., Kritzinger, J., Bauer, W., Preston, J., The Influence of Application System on the Structure of Coating Layer, 2010 Tappi Coating Conference Proceedings.
2. Gane, P., Hooper, J., Grunwald, A., Coating pigment orientation: A comparative analysis of the application mechanisms and properties of blade and roll coatings, Tappi Journal; Vol. 80, No, 2, pp 109 – 112.
3. Carlsson, J., Eckl, J., Reimers, O., A Comparison of Metering Elements for Producing Double-Coated Paperboard.
4. Parker, Q., Aqueous gluing of coated paperboard packaging products in North America, Tappi Journal Solutions Online Exclusives, April 2004.
5. Trudelle, C., Poustis, J., Measurement of Glue on Corrugated Board by Fluorescence X-ray, 1993 International Corrugated Containers Conference, pp. 35 – 48.
6. Xu, R., Pekarovicova, A., Fleming, P., Bliznyuk, V., Physical Properties of LWC Papers and Gravure Ink Mileage, Proceedings 2005 Tappi Coating Conference, p. 365.
7. Ozaki, Y., Bousfield, D.W., Shaler, S.M., Three-Dimensional Characterization of Ink Vehicle Penetration by Laser scanning Confocal Microscopy, J. Pulp Paper Sci, 2005, pp. 48 – 52.

8. Ozaki, Y., Bousfield, D.W., Shaler, S.M., Observation of the Ink Penetration in the Coated Paper by Confocal Laser Scanning Microscope. TAGA J., Vol. 3, 50.
9. Ozaki, Y., Bousfield, D.W., Shaler, S.M., Three Dimensional Observation of Coated Paper by Laser Scanning Confocal Microscopy, Tappi Journal, 5(2), 3.
10. Erdman, N., Campbell, R., Asahina, S., Precise SEM Cross Section Polishing via Argon Beam Milling, Microscopy Today, May 2006, pp. 22 – 25.

APPENDIX A:

Basecoat	**BC Run**	**1**	**2**	**3**	**4**	**5**	**6**	**10**	**11**	**12**	**13**	**14**	**15**	**28**	**29**	**30**
	BC Ctr	Blade	Blade	Blade	Blade	Blade	Blade	Rod	Rod	Rod	Rod	Rod	Rod	FC	FC	FC
	BC Ash lbs/MSF	2.9	2.7	1.7	3.2	2.6	1.5	3.6	2.4	1.9	2.7	2.1	1.6	2.9	2.7	1.9
TopCoat	**TC Run**	**7**	**8**	**9**	**31**	**32**	**33**	**22**	**23**	**24**	**34**	**35**	**36**	**40**	**41**	**42**
	TC Ctr	Blade	Blade	Blade	AK	AK	AK	Rod	Rod	Rod	AK	AK	AK	AK	AK	AK
	TC Ash lbs/MSF	2.0	2.2	3.1	2.6	2.5	3.1	1.4	2.6	2.6	3.1	2.9	3.2	2.4	2.0	3.3
	Total CtWt #/MSF	4.9	4.9	4.8	5.8	5.1	4.6	5.0	5.0	4.5	5.8	5.0	4.8	5.3	4.7	5.2
AQ Glue 0.5hr	% fibre tear	5.0	5.0	12.5	0.0	0.0	41.7	0.0	0.0	0.0	0.0	0.0	0.0	0.0	5.0	28.3
AQ Glue 1hr	% fibre tear	100.0	100.0	97.5	57.5	36.7	97.5	95.0	87.5	7.5	45.0	28.3	40.0	68.3	100.0	100.0
AQ Glue 2hr	% fibre tear	100.0	100.0	100.0	97.5	85.0	100.0	95.0	60.0	82.5	90.0	73.3	92.5	100.0	100.0	100.0
Hot Melt Glue Test %Tear	% fibre tear	100.0	61.7	92.5	87.5	55.0	100.0	40.0	50.0	30.0	72.5	60.0	50.0	71.7	60.0	95.0
Delta Glue (AQ 2hr - Hot Melt)	% fibre tear	0.0	38.3	7.5	10.0	30.0	0.0	55.0	10.0	52.5	17.5	13.3	42.5	28.3	40.0	5.0
Hagerty Porosity Basecoat	sec/10cc	440.0	422.0	339.0	420.0	416.4	344.7	326.5	293.8	256.0	327.7	285.0	249.8	144.7	131.9	123.7
Hagerty Porosity Topcoat	sec/10cc	699.6	692.0	763.6	826.0	819.2	730.4	596.4	563.6	584.4	651.2	589.6	567.2	463.2	470.8	447.2
Emtec Base Slope	Intensity/sec	-3.0	-3.1	-3.3	-2.9	-2.9	-3.2	-3.3	-3.4	-3.3	-3.0	-2.9	-3.0	-3.2	-3.8	-4.2
Emtec Top Slope	Intensity/sec	-3.1	-2.7	-2.7	-3.0	-2.4	-2.7	-2.3	-3.1	-2.8	-3.5	-2.9	-2.5	-2.4	-2.2	-2.4
BasecoatBristow 0.14sec	cm^3/m^2	1.73	2.50	2.90	2.61	3.06	2.59	4.17	3.97	4.29	3.48	3.38	3.30	4.23	4.99	5.60
Basecoat Bristow 0.32sec	cm^3/m^2	1.93	3.57	4.82	4.63	4.08	4.67	5.71	5.50	5.55	5.12	4.60	4.94	5.82	6.92	6.84
Basecoat Bristow 1.0sec	cm^3/m^2	2.03	9.05	9.34	9.80	9.19	8.91	9.80	9.80	9.80	9.97	8.91	9.19	12.25	12.52	13.37
Topcoat Bristow 0.14sec	cm^3/m^2	1.78	2.26	1.99	1.77	2.10	2.31	3.70	2.55	2.70	3.32	2.50	2.74	3.38	2.93	3.50
Topcoat Bristow 0.32sec	cm^3/m^2	2.58	2.50	2.64	3.21	3.00	3.59	3.97	3.65	3.68	4.06	3.77	3.72	4.90	4.52	5.60
Topcoat Bristow 1.0sec	cm3/m2	8.17	8.06	7.64	7.64	7.45	8.29	8.65	8.78	8.29	9.19	8.40	8.29	9.34	9.64	10.14
Sheet Gloss		28.4	32.2	42.2	34.3	34.9	28.6	38.8	43.9	44.0	36.4	35.0	32.0	31.1	28.8	25.2
Ink Gloss		63.0	64.6	75.7	65.0	61.0	51.2	51.9	60.4	64.7	58.9	57.1	51.2	50.4	48.3	44.1
Delta Gloss		34.6	32.4	33.5	30.8	26.1	22.5	13.1	16.5	20.7	22.6	22.0	19.1	19.3	19.5	18.9
GE Brightness		85.1	85.3	85.8	86.4	86.1	86.3	85.8	86.1	86.3	86.3	86.1	86.3	86.3	86.4	86.6
PPS Basecoat	micron	2.00	2.07	2.68	1.89	1.93	2.69	2.94	2.60	3.00	3.05	2.71	3.10	4.21	4.57	4.52
PPS Topcoat	micron	1.11	1.24	1.11	1.74	1.68	2.40	2.37	2.00	2.05	2.47	2.06	2.36	2.87	2.69	2.79
Deltack Slope	N/m-sec	2.65	3.22	2.74	2.16	1.98	1.55	1.80	2.01	2.03	1.90	1.86	1.61	1.65	1.60	1.38
Deltack Force at Failure	N/m	53.6	54.0	52.2	49.0	49.0	42.4	35.0	38.3	38.1	42.4	43.7	42.6	33.3	37.5	37.1
Deltack Passes to Pick		6.0	5.0	5.0	6.0	6.5	7.0	5.0	5.0	5.0	6.0	6.0	7.0	5.5	6.0	6.5
IGT Dry Pick	ft/min	309.0	335.3	315.5	335.7	331.0	324.0	301.0	340.7	314.7	395.7	336.5	363.0	403.0	403.0	368.0
Halftone Papeye Mottle		6.5	6.1	5.9	5.9	5.5	6.5	5.7	5.6	5.5	5.7	5.9	6.3	6.8	7.2	7.0
Fulltone Papeye Mottle		1.2	2.3	1.2	1.5	1.1	1.4	1.2	1.0	1.0	1.2	1.3	1.3	1.4	1.4	1.8
Flexo Dot Gain 50%	%	22.9	22.5	20.9	23.2	22.6	22.8	22.2	21.0	22.0	23.3	22.5	22.7	24.7	24.4	23.7
Helio	mm to 20 missing dots	110.0	110.0	110.0	110.0	110.0	88.8	35.8	36.2	50.2	83.5	90.3	79.2	25.5	29.8	35.3
Wet Repell. Dry Density		0.906	0.885	0.942	0.948	0.965	0.935	0.937	0.948	0.953	0.955	0.956	0.943	0.908	0.922	0.911
Wet Repell. Wet Density		0.691	0.687	0.673	0.804	0.832	0.744	0.722	0.728	0.713	0.800	0.830	0.783	0.767	0.774	0.677
Delta Density		0.214	0.198	0.269	0.143	0.133	0.191	0.215	0.220	0.240	0.155	0.126	0.160	0.141	0.148	0.234
Wet Pick	Brightness	19.4	15.0	27.1	9.5	6.2	8.9	25.1	23.0	26.2	12.4	7.9	11.2	9.1	8.8	16.9